ACS APPLIED MATERIALS & INTERFACES

Research Article

www.acsami.org

Theoretical Understanding and Prediction of Lithiated Sodium Hexatitanates

Yun Wang,[†] Haimin Zhang,[†] Xiangdong Yao,[‡] and Huijun Zhao*,[†]

[†]Centre for Clean Environment and Energy, and Griffith School of Environment, Griffith University, Gold Coast, QLD 4222, Australia

[‡]QLD Micro- and Nanotechnology Centre, Nathan Campus, Griffith University, QLD 4111, Australia

Supporting Information

ABSTRACT: Sodium hexatitanates ($Na_2Ti_6O_{13}$) with tunnelled structures have been experimentally proposed to be good candidates for anode materials of lithium ion batteries because of their low potential, small shape transformation, and good reversibility. The understanding of the properties of this lithiated titanate is significant for their development. To this end, the first-principle calculations were performed to investigate the interaction between Li ions and $Na_2Ti_6O_{13}$ at the atomic level. After structural optimization with various Li:Ti ratios, the Li ions are found to energetically prefer to stay at the small rhombic tunnels of $Na_2Ti_6O_{13}$, where the diffusion energy barrier of Li ions is also lower. Such preference is determined by the chemical environment around Li ions. Our theoretical intercalation potential and volume change on the basis of the optimized atomic structures agree with the experimental observations. The analysis of the electronic properties reveals the Burstein–Moss effect in lithiated $Na_2Ti_6O_{13}$ due to the heavy n-type doping. Such materials possess high conductivity, which can benefit their applications in photoelectrochemical or electrochemical areas.

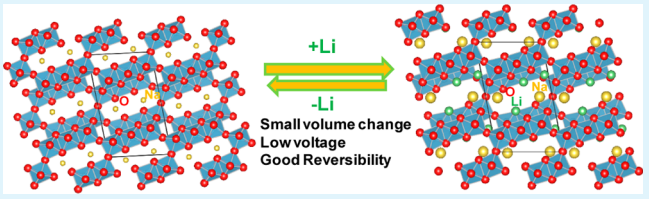

KEYWORDS: *anode of lithium ion battery, lithiated titanate, intercalation mechanism, density functional theory, Burstein–Moss effect, photocatalysis*

1. INTRODUCTION

Lithium-ion batteries (LIB) represent serious candidates to store energy in term of their volumetric and specific energy density to deal with the current environment and energy related crisis.[1,2] The screen of the high-performance electrode materials for LIB is one of the key issues for their development. The criteria of a good anode material for LIB include low voltage ranges and small volume distortion during charge–discharge cycling. Ti–O-based materials have been previously demonstrated to satisfy these requirements.[3−6] For example, lithium titanates with a spinel structure ($Li_4Ti_5O_{12}$) have been found to be a "zero strain" anode material.[7,8] The voltage range of these Ti–O-based materials is within 1.5 − 2.0 V.[9] Consequently, various Ti–O based materials have already been explored as potential anode materials for LIB. These materials include pure titanium oxides (TiO_2) with anatase, rutile, or TiO_2–B structure, $Li_4Ti_5O_{12}$, and $Li_2Ti_3O_7$.[5,6,9,10]

Recently, sodium hexatitanates ($Na_2Ti_6O_{13}$) have been proposed to be good anode materials of LIB since their voltage range for the reversible insertion of lithium ions is 1.0–1.5 V, which is lower than the other Ti–O-based materials.[11,12] The volume expansion is just about 2% when Li intercalates into $Na_2Ti_6O_{13}$. At the same time, sodium titanates can be readily produced in large quantity via facile hydrothermal processes.[13−15] However, due to the limit of experiments, the origin of these advantages is unclear. The atomic understanding of the physicochemical properties of LIB electrode materials has been demonstrated to be useful to improve their performance successfully.[16,17] In this regard, the first-principle theoretical study was dedicated to investigate the lithiated $Na_2Ti_6O_{13}$ materials. The effect of the Li intercalation on the electronic structures of titanates was also discussed.

2. COMPUTATION METHODS

The $Na_2Ti_6O_{13}$ systems with or without intercalated Li ions were investigated using the Vienna ab initio simulation program (VASP) based on the first-principle density functional theory (DFT) with the all-electron projected augmented wave (PAW) method in this study.[18−20] A plane-wave basis set was employed with a kinetic energy cut-off of 500 eV. For the electron-electron exchange and correlation interactions, the functional of Perdew, Burke and Ernzerhof (PBE),[21] a form of the general gradient approximation (GGA), was used throughout. The GGA functional was employed due to its better performance in calculations than the local density approximation (LDA) functional.[21,22] This is because the GGA methods add a dependence on the gradients of the spin densities. The supercell of $Na_2Ti_6O_{13}$ used in this study includes 42 atoms. When the structures were optimized, all atoms were allowed to relax. Since there were several structure parameters to determine the optimized lattices of the systems, to obtain the theoretical values of these parameters through traditional DFT calculations was very time-consuming. Thus, the

Received: November 29, 2012
Accepted: January 18, 2013
Published: January 18, 2013

   dx.doi.org/10.1021/am302907v | ACS Appl. Mater. Interfaces 2013, 5, 1108–1112

variable cell technique was employed to optimize these lattice parameters. The structures were optimized until the residual forces were below 0.001 eV/Å. We performed Brillouin-zone integrations using Monkhorst-Pack grids of special points with a (1× 4 × 2) mesh for $Na_2Ti_6O_{13}$. The selected *k*-mesh densities and the cut-off kinetic energy have been justified in our previous studies.[23−26]

To compare the stability of various configurations, the interaction energy (ΔE) of Li with $Na_2Ti_6O_{12}$ was calculated by the equation

$$\Delta E = (E_{Li_xNa_2Ti_6O_{13}} - xE_{Li} - E_{Na_2Ti_6O_{13}})/x$$

where the energies of Li and $Na_2Ti_6O_{13}$ with or without intercalated Li were from their average energy in bulk calculations. The x is the number of Li intercalated into the crystal. The average energy of Li bulk was calculated by using a (16 × 16 × 16) k-point mesh.

3. RESULTS AND DISCUSSION

3.1. $Na_2Ti_6O_{13}$ Crystal. $Na_2Ti_6O_{13}$ is a typical alkali metal titanate with a basic formula $A_2Ti_nO_{2n+1}$, which exhibit a tunnelled structure with a large specific area. The $Na_2Ti_6O_{13}$ crystal is a monoclinic cell with space group *C2/m*.[27] Our optimized structure of $Na_2Ti_6O_{13}$, listed in Table 1, agreed with the previous theoretical and experimental data,[26,27] which, in turn, demonstrated that the calculation parameters used in this study were reliable. Figure 1 shows the optimized atomic structures of $Na_2Ti_6O_{13}$ crystal. It can be found that there are two different sizes of tunnels: the big one is an 8.4 Å × 2.7 Å quasi-rectangle (in the blue frame of Figure 1), which accommodates two Na atoms in each unit; and the side length of the small rhombic ones is about 3.0 Å (in the green frame of Figure 1), which is similar as those in anatase TiO_2.[26]

Table 1. Theoretical Lattice Constants of $Na_2Ti_6O_{13}$ in Comparison with the Previous Theoretical[26] and Experimental Data[27]

	this work	theo.[26]	exp.[27]
a (Å)	15.27	15.21	15.10
b (Å)	3.76	3.75	3.75
c (Å)	9.29	9.25	9.17
β (deg)	99.1	98.9	99.0
V (A^3)	526.4	520.8	512.3

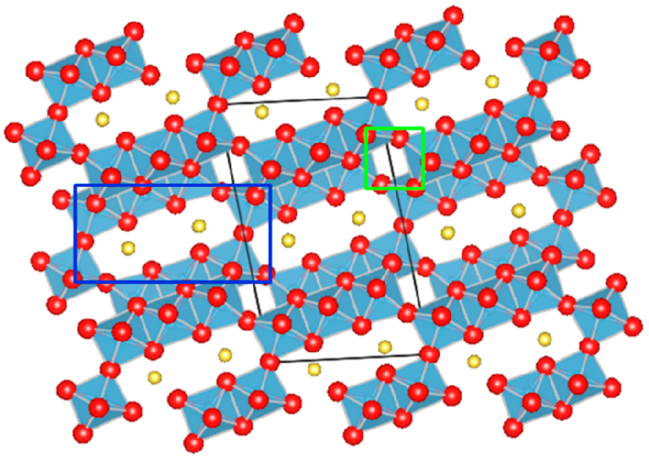

Figure 1. Atomic configuration of $Na_2Ti_6O_{13}$ materials with two tunnels. The black rhombic frame represents the size of a unit cell. The Blue frame shows the area of big quasi-rectangular tunnel. And the green frame indicates the location of the small rhombic tunnel. Key: blue octahedron, [TiO_6]; yellow, sodium; red, oxygen; blue, titanium.

3.2. Low Li Concentration. When Li concentration is low, the configurations including one Li ion per $Na_2Ti_6O_{13}$ unit with the Li:Ti ratio as 1/6 are employed to simulate the systems. Three stable configurations have been found after the structural optimization, as shown in Figure 2. In the configuration 2A, the Li ion intercalates into the small rhombic tunnel. The Li ion locates at the centre of the big quasi-rectangular tunnel in the configuration 2B. In the configuration 2C, the Li ion is at the edge of the big quasi-rectangular tunnel. The stabilities of these three configurations are compared through their ΔE between Li ions and $Na_2Ti_6O_{13}$, which are listed in Figure 2. The configuration 2A is the most stable one among three systems according to our calculations. This can be ascribed to the different numbers of lattice oxygen atoms around the Li ion. In configuration 2A, each Li ion bonds with five oxygen atoms. As a comparison, each Li ion in the other two configurations interacts with four oxygen atoms. Consuently, the Li ion in the small rhombic tunnels associates with one more oxygen atom, which stengthens the interaction between Li ions and $Na_2Ti_6O_{13}$.

The stronger Li−O interaction in configuration 2A can be further supported by the analysis of the partial density of states (PDOS) of Li atoms. From Figure 2, the area of non-bonding band of Li atoms around Fermi energy level in the configuration 2A is the smallest. This indicates that there is more hybridization between the Li 2s and O 2p orbitals in the configuration 2A. As a result, the area of bonding bands of the Li atoms in the configuration 2A becomes larger in the energy area less than −3.0 eV. Although the coordination number of Li atoms in configurations 2B and 2C are same, their PDOS images vary. The density of nonbonding bands of Li atoms in the configuration 2B is higher than that in the configuration 2C. Correspondingly, the density of bonding bands of Li atoms in the configuration 2C is higher. Such differentia suggests that there is a stronger Li−O interaction in the configuration 2C than that in the configuration 2B. However, the ΔE of 2B is 0.57 eV lower than that of 2C. This can be explained by considering the change of the volume after Li intercalation. According to our calculations, the volume change in configuration 2C is almost four times larger than that in configuration 2B. Thus, the intercalation of Li in the configuration 2C leads to much significant strain, which reduces the stability of the systems.

In the most stable configuration 2A, the Li intercalation expands the volume of titanates by 1.80%. The theoretical value is close to the experimental meansurement through in situ XRD, which is about 2.0%.[11] Thus, from the structural view, it also supports that Li ions prefer to intercalate into the relatively small rhombic channnel when the concentration of Li is small.

3.3. Lithium Diffusion. The diffusion of intercalated Li ions is important for LIB since it determines the power output and battery charging times. Therefore, the diffusion energy barriers of Li ions in the tunnels of $Na_2Ti_6O_{13}$ were calculated using the nudged elastic band (NEB) method in this study.[28] The Li ions diffuse along the direction of tunnels (see Figure 3). Because the diffusion path needs be within one supercell using the NEB approach, a (1 × 2 × 1) supercell was employed to simulate the diffusion path of Li ions between the neighboring unit cells. Under this situation, the Li:Ti ratio is 1/12. The volume changes of these lithiated titanates are expected to be neglectable since the volume changes of the

dx.doi.org/10.1021/am302907v | ACS Appl. Mater. Interfaces 2013, 5, 1108−1112

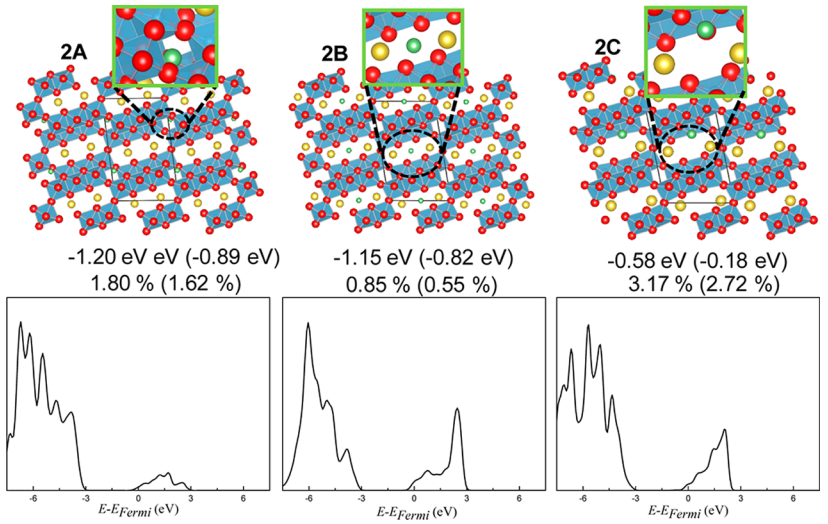

Figure 2. Atomic configurations of $Li_1Na_2Ti_6O_{13}$ materials with different locations of Li (upper) and the partial density of states of Li atoms in the corresponding configurations (lower). The inset images show the detailed atomic structures around Li. The average interaction energy of Li with $Na_2Ti_6O_{13}$ and the percentage of volume change with GGA calculations are also listed. The values in the brackets are calculated using GGA+U approach. The black rhombic frame represents the size of a unit cell. Key: blue octahedron, [TiO_6]; yellow, sodium; red, oxygen; blue, titanium; green, lithium.

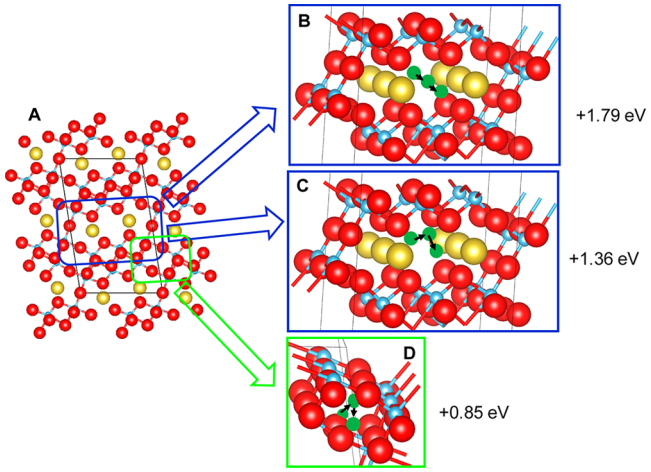

Figure 3. Atomic configurations of (A) $Na_2Ti_6O_{13}$ and (B–D) three diffusion paths of Li ions with the Li:Ti as 1/12. The black rhombic frame in A represents the size of a unit cell. The areas in the blue rectangles of A–C are the big quasi-rectangle tunnels of $Na_2Ti_6O_{13}$. And the areas in the green rectangles of A and D are the small rhombic tunnels of $Na_2Ti_6O_{13}$. The related diffusion energy barriers are also listed on the basis of the GGA calculations. Key: yellow, sodium; red, oxygen; blue, titanium; green, lithium.

optmized configurations with Li:Ti ratio as 1/6 are less than 2% in the configuration 2A or 2B, as discussed above. Consequently, we investigated the Li diffusion energy barriers using the lattice constants of bare $Na_2Ti_6O_{13}$ without consideration of the volume change.

Because of the specific tunnelled structure, the diffusion energy barriers of Li ions in the big quasi-rectangle tunnels are expected to be low and firstly investigated. Considering that the intercalation of Li ions with the configuration 2C is energetically unfavorable, Li ions locate at the centres of the big quasi-rectangle tunnel in the initial and final stage of our considerred diffusion paths. Suprisingly, the energy barrier is relatively high, 1.79 or 1.36 eV when Li ions move right through the centre of two Na ions or above the Na ions, respectively, as shown in Figure 3B, C. As a comparison, the diffusion barrier of Li ions in anatase TiO_2 materials is just about 0.6 eV.[29] Thus, the diffusion rate of Li ions in the big quasi-rectangle tunnels is slow.

The diffusion of Li ions in small rhombic tunnels is also calculated (see Figure 3D). The energy barrier is 0.85 eV, which is at least 37.5% less than those in the big quasi-rectangle. Thus, it demonstrates that the diffusion rates of Li ions are not determined the size of tunnels. From Figure 1, there is no Na ions in the small rhombic tunnels of $Na_2Ti_6O_{13}$. As a result, there is no Li–Na elestrostatic repulsion when Li ions diffuse in these tunnels. In addition, the energy barrier is lower when Li ions diffuse along the path shown in Figure 3C comparing with that in Figure 3B. The main difference between these two diffusion path is the Li–Na distance in the intermediate. The shoter Li–Na distance in Figure 3C leads to the stronger Li–Na electrostatic repulsion, which further increase the diffusion energy barrier. Consequently, the Li–Na electrostatic repulsion is found to determine the diffusion rates of Li ions in $Na_2Ti_6O_{13}$. According to this deduction, using hydrogen atoms to replace partial Na atoms may increase the diffusion rate of Li ions in the big quasi-rectangle tunnels of titanates.[23,30] Because the smallest diffusion energy barriers of Li ions in $Na_2Ti_6O_{13}$ are close to those in anatase TiO_2, the similar power output and battery charging times of these two materials are expected when the concentration of Li ions is low.

3.4. High Li Concentration. When the Li concentration becomes higher, multiple Li ions can be in one $Na_2Ti_6O_{13}$ unit. From the experiments, the maximum number of Li ions intercalating into each $Na_2Ti_6O_{13}$ unit is three.[11] Thus, the configurations with two or three Li ions per $Na_2Ti_6O_{13}$ unit were theoretically investigated. When Li:Ti ratio is 1/3 (two Li ions per $Na_2Ti_6O_{13}$ unit), two configurations have been found to be energetically allowed in this study, as shown in Figure 4. The Li ions intercalate into the big and small tunnels simultaneously in the configuration 4A. The Li ions in the big quasi-rectangular tunnels locate at their centres. In the configuration 4B, both Li ions locate at the edge of the big quasi-rectangular tunnel. Such accommodation not only

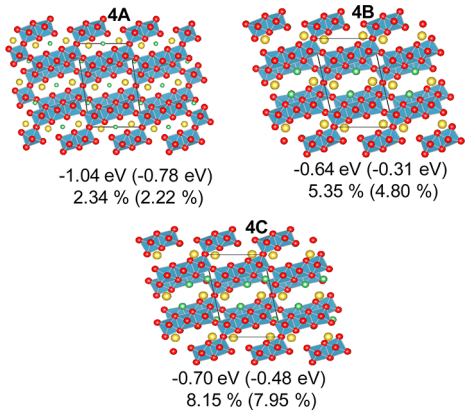

Figure 4. Atomic configurations of (A, B) $Li_2Na_2Ti_6O_{13}$ and (C $Li_3Na_2Ti_6O_{13}$) materials with different locations of Li. The average interaction energy of Li with $Na_2Ti_6O_{13}$ and the percentage of volume change with GGA calculations are also listed. The values in the brackets are calculated using GGA+U approach. The black rhombic frame represents the size of a unit cell. Key: blue octahedron, [TiO_6]; yellow, sodium; red, oxygen; blue, titanium; green, lithium.

increases the electrostatic repulsion between the metallic ions, but also enhances the strain of the systems. In the configuration 4B, the volume expands 5.35%. As a comparison, the volume increases just by 2.34% in the configuration 4A. Meanwhile, the Li ions at the edge of big quasi-rectangular tunnel are not energetically preferred (see Figure 2C). Consequently, the configuration 4A is more stable when two Li ions intercalate into $Na_2Ti_6O_{13}$.

When Li:Ti ratio reaches 1/2 (three Li ions per $Na_2Ti_6O_{13}$ unit), only one stable configuration was obtained as shown in Figure 4C. In this structure, one Li locates at the small rhombus tunnnel; and the other two Li locate at the edge of the big quasi-rectangular tunnel in each $Na_2Ti_6O_{13}$ unit. Under this condition, the volume of titanate crystal increase by 8.15%, which is much larger than those when the concentrations of Li ions are low. However, Figure 4 reveals that the Ti−O-based frameworks are not destroyed even when the concentration of Li ion is high. This can be ascribed to the specific tunnelled structures of $Na_2Ti_6O_{13}$. Consequently, $Na_2Ti_6O_{13}$ shows good structural reversibility during the charge−discharge cycling, as found in the experiments.[11]

3.5. Intercalation Voltage. The experimental potential values of the lithiated $Na_2Ti_6O_{13}$ are 1.35 V and 1.12 V found in cyclic voltamogram measurement.[11] Our corresponding theoretical potential is 1.20 V for Li intercalation into $Na_2Ti_6O_{13}$, or 0.89 V for Li intercalation into $Li_1Na_2Ti_6O_{13}$. The previous studies have demonstrated that the GGA+U calculations can predict the intercalation potential into TiO_2 more accurately.[29,31] Following a previous study, we chose U-J as 4.2 eV for Ti to recalculate the potentials of Li intercalation into $Na_2Ti_6O_{13}$ or $Li_1Na_2Ti_6O_{13}$. All the GGA+U results have been shown in Figures 2 and 4. The GGA+U potentials are 0.82 V and 0.76 V for Li intercalation into $Na_2Ti_6O_{13}$ and $Li_1Na_2Ti_6O_{13}$, respectively. Both GGA and GGA+U data suggest that the current experimental potentials are higher than theoretical ones. The further optimization of the synthesis parameters may reduce their potentials to improve their performance as anode materials of LIB.

3.6. Electronic Structures. Because titanates have also been proposed to be used in photocatalysis,[14,32,33] the electronic structures of $Na_2Ti_6O_{13}$ with and without intercalated Li are compared. The locations of the conduction band minimum (CBM) and valence band maximum (VBM) related to the Fermi energy level are illustrated in Figure 5 on the basis

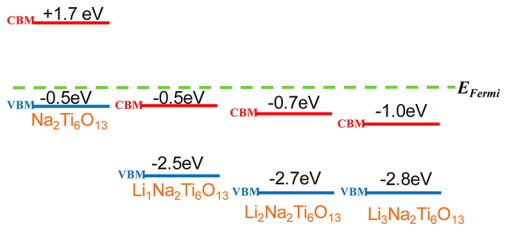

Figure 5. Illustration of the relative position of conduction band minimum (CBM) and valence band maximum (VBM) of $Na_2Ti_6O_{13}$, $Li_1Na_2Ti_6O_{13}$, $Li_2Na_2Ti_6O_{13}$, and $Li_3Na_2Ti_6O_{13}$ comparing with the Fermi energy level.

of the DOS calculations. After Li intercalation, both CB and VB bands bend to the lower energy level, which means that lithiated titanates are n-type semiconductors. Meanwhile, the Burstein-Moss shift is discovered since the Fermi energy levels lie inside the CB in the lithiated titanates. The Burstein−Moss effect is led by the heavy n-type doping of Li, which pushes Fermi level higher in energy.[34] Correspondingly, this shift increases with the concentration of Li, as shown in Figure 5. The existence of occupied donor states around the Fermi energy level can increase the conductivity of systems, which can benefit the performance in photocatalysts and electrochemistry.[35] The prediction of the n-type conductivity needs to be further verified by the experiments.

4. CONCLUSION

In this study, the lithiated $Na_2Ti_6O_{13}$ was theoretically investigated through first-principle DFT calculations. After the optimization of their structures, it is found that the Li ions prefer intercalating into the small rhombic tunnel of $Na_2Ti_6O_{13}$ initially since Li atoms can interact with more lattice oxygen atoms there. At the same time, the lack of Li−Na electrostatic repulsion in the small rhombic tunnels of titanates leads that Li ions diffuse there more quickly. The intercalation of Li increase the volume of $Na_2Ti_6O_{13}$ by 1.80−2.34 % when the Li:Ti ratio is less than 1/3. The small volume changes are in line with the experimental observation that solid solution type evolution occured. Our optimized structures demonstrate that the Ti−O based frameworks are kept after the Li intercalation ascribed to the specific tunnelled structures of $Na_2Ti_6O_{13}$. As a result, the Li intercalation is structurally reversible. Meanwhile, our theoretical intercalation potentials are 1.20 V and 0.89 V, which are lower than those of the other Ti−O based anode materials. The theoretical low potentials, less volume changes, and good reversibility found in this study confirm that $Na_2Ti_6O_{13}$ is a good anode for LIB. The further analysis on their electronic structures indicates that lithiated titanates possess n-type conductivity, which can benefit their electrochemiscal and photoelectrochemical appications. Because $Na_2Ti_6O_{13}$ is a representative of tunnelled alkali metal titanates, other titanates with the similar structures are expected to be also good candidates for anode materials of LIB.

■ ASSOCIATED CONTENT

Ⓢ Supporting Information

Corresponding atomic coordinates. This material is available free of charge via the Internet at http://pubs.acs.org

AUTHOR INFORMATION

Corresponding Author

*Tel: (+) 61-7-55528261. Fax: (+) 61-7-55528067. E-mail: h.zhao@griffith.edu.au.

Notes

The authors declare no competing financial interest.

ACKNOWLEDGMENTS

We thank the Australian Research Council for funding this work. This research was undertaken on the National Computation Infrastructure (NCI) in Canberra, Australia.

REFERENCES

(1) Armand, M.; Tarascon, J. M. *Nature* **2008**, *451*, 652−657.
(2) Wagner, F. T.; Lakshmanan, B.; Mathias, M. F. *J. Phys. Chem. Lett.* **2010**, *1*, 2204−2219.
(3) Zhu, G. N.; Wang, Y. G.; Xia, Y. Y. *Energy Environ. Sci.* **2012**, *5*, 6652−6667.
(4) Yin, S. Y.; Song, L.; Wang, X. Y.; Huang, Y. H.; Zhang, K. L.; Zhang, Y. X. *Electrochem. Commun.* **2009**, *11*, 1251−1254.
(5) Jiang, C. H.; Wei, M. D.; Qi, Z. M.; Kudo, T.; Honma, I.; Zhou, H. S. *J. Power Sources* **2007**, *166*, 239−243.
(6) Yang, Z. G.; Choi, D.; Kerisit, S.; Rosso, K. M.; Wang, D. H.; Zhang, J.; Graff, G.; Liu, J. *J. Power Sources* **2009**, *192*, 588−598.
(7) Amatucci, G. G.; Badway, F.; Du Pasquier, A.; Zheng, T. *J. Electrochem. Soc.* **2001**, *148*, A930−A939.
(8) Ferg, E.; Gummow, R. J.; de Kock, A.; Thackeray, M. M. *J. Electrochem. Soc.* **1994**, *141*, L147−L150.
(9) Zhou, W. J.; Liu, H.; Boughton, R. I.; Du, G. J.; Lin, J. J.; Wang, J. Y.; Liu, D. *J. Mater. Chem.* **2010**, *20*, 5993−6008.
(10) Bavykin, D. V.; Friedrich, J. M.; Walsh, F. C. *Adv. Mater.* **2006**, *18*, 2807−2824.
(11) Dominko, R.; Baudrin, E.; Umek, P.; Arcon, D.; Gaberscek, M.; Jamnik, J. *Electrochem. Commun.* **2006**, *8*, 673−677.
(12) Dominko, R.; Dupont, L.; Gaberscek, M.; Jamnik, J.; Baudrin, E. *J. Power Sources* **2007**, *174*, 1172−1176.
(13) Liu, P. R.; Zhang, H. M.; Liu, H. W.; Wang, Y.; Yao, X. D.; Zhu, G. S.; Zhang, S. Q.; Zhao, H. J. *J. Am. Chem. Soc.* **2011**, *133*, 19032−19035.
(14) Riss, A.; Elser, M. J.; Bernardi, J.; Diwald, O. *J. Am. Chem. Soc.* **2009**, *131*, 6198−6206.
(15) Zhu, H. Y.; Lan, Y.; Gao, X. P.; Ringer, S. P.; Zheng, Z. F.; Song, D. Y.; Zhao, J. C. *J. Am. Chem. Soc.* **2005**, *127*, 6730−6736.
(16) Ceder, G. *Science* **1998**, *280*, 1099−1100.
(17) Kang, K. S.; Meng, Y. S.; Breger, J.; Grey, C. P.; Ceder, G. *Science* **2006**, *311*, 977−980.
(18) Kresse, G.; Hafner, J. *Phys. Rev. B* **1993**, *47*, 558−561.
(19) Kresse, G.; Furthmuller, J. *Comput. Mater. Sci.* **1996**, *6*, 15−50.
(20) Kresse, G.; Joubert, D. *Phys. Rev. B* **1999**, *59*, 1758−1775.
(21) Perdew, J. P.; Burke, W.; Ernzerhof, M. *Phys. Rev. Lett.* **1996**, *77*, 3865−3868.
(22) Cramer, C. J.; Truhlar, D. G. *Phys. Chem. Chem. Phys.* **2009**, *11*, 10757−10816.
(23) Wang, Y.; Liu, H. W.; Zhang, H. M.; Yao, X. D.; Zhao, H. J. *Chem. Phys. Lett.* **2011**, *511*, 82−86.
(24) Wang, Y.; Hwang, G. S. *Surf. Sci.* **2003**, *542*, 72−80.
(25) Wang, Y.; Zhang, H. M.; Han, Y. H.; Liu, P. R.; Yao, X. D.; Zhao, H. J. *Chem. Commun.* **2011**, *47*, 2829−2831.
(26) Wang, Y.; Sun, T.; Yang, D. J.; Liu, H. W.; Zhang, H. M.; Yao, X. D.; Zhao, H. J. *Phys. Chem. Chem. Phys.* **2012**, *14*, 2333−2338.
(27) Torres-Martinez, L. M.; Juarez-Ramirez, I.; Del Angel-Sanchez, K.; Garza-Tovar, L.; Cruz-Lopez, A.; Del Angel, G. *J. Sol−Gel Sci. Technol.* **2008**, *47*, 158−164.
(28) Henkelman, G.; Johannesson, G.; Jonsson, H., Methods for Finding Saddle Points and Minimum Energy Paths. In *Theoretical Methods in Condensed Phase Chemistry*; Kluwer: Dordrecht, The Netherlands, 2000; Vol. *5*, pp 269−302.
(29) Morgan, B. J.; Watson, G. W. *Phys. Rev. B* **2010**, *82*, 144119.
(30) Liu, H. W.; Yang, D. J.; Zheng, Z. F.; Ke, X. B.; Waclawik, E.; Zhu, H. Y.; Frost, R. L. *J. Raman Spectrosc.* **2010**, *41*, 1331−1337.
(31) Morgan, B. J.; Watson, G. W. *J. Phys. Chem. Lett.* **2011**, *2*, 1657−1661.
(32) Inoue, T.; Fujishima, A.; Konishi, S.; Honda, K. *Nature* **1979**, *277*, 637−638.
(33) Inoue, Y.; Kubokawa, T.; Sato, K. *J. Chem. Soc.−Chem. Commun.* **1990**, 1298−1299.
(34) Grundmann, M. *The Physics of Semiconductors: An Introduction Including Devices and Nanophysics*; Springer-Verlag: Berlin, 2006; pp 235−236.
(35) Vittadini, A.; Schirmer, M.; Walz, M. M.; Vollnhals, F.; Lukasczyk, T.; Steinruck, H. P.; Marbach, H.; Riss, A.; Elser, M. J.; Schurer, B.; et al. *Langmuir* **2012**, *28*, 7851−7858.